Check for updates

Systematic characterization of metabolic profiles of ingenol in rats by UPLC-Q/TOF-MS and NMR in combination with microbial biotransformation†

Si-Jia Xiao, [iD] ‡[a] Shan-Shan Li,‡[b] Bin Xie,[a] Wei Chen,[a] Xi-Ke Xu,[a] Xian-Peng Zu*[a] and Yun-Heng Shen [iD] *[a]

Ingenol, as the precursor of the marketed drug ingenol mebutate, has been proven to have a variety of bioactivities. The purpose of this study was to identify the metabolites of ingenol using ultra-performance liquid chromatography-quadrupole time-of-flight-mass spectrometry (UPLC-Q/TOF-MS) combined with UNIFI software. Plasma, urine and fecal samples of rats were obtained and analyzed. A total of 18 metabolites were detected and identified in rat, including five phase II metabolites (**M14–M18**). Moreover, as microbial biotransformation is helpful to obtain sufficient reference standards of metabolites, the co-culture of ingenol with the fungus *Cunninghamella elegans* bio-110930 was also studied and yielded 4 phase I metabolites, in which reference standards of three metabolites were further obtained by preparative scale biotransformation. By matching their retention times, accurate masses, and fragment ions with metabolites in rat, the structures of three metabolites (**M2**, **M3** and **M4**) were unambiguously confirmed by NMR technology. The results revealed that *C. elegans* bio-110930 functioned as an appropriate model to mimic and prepare phase I metabolism of ingenol *in vivo* to a certain extent. It also revealed that hydroxylation, oxygenation, sulfonation, and glucuronidation were the major metabolic pathways of ingenol. Furthermore, the first systematic metabolic study of ingenol is of great significance to elucidate the metabolites and metabolic pathways *in vivo*, which is helpful to predict metabolites of ingenol in humans, understand the elimination mechanism of ingenol, and clarify its effectiveness and toxicity.

Introduction

Ingenol (Fig. 1), a natural ingenane type of diterpenoid, is one of the active ingredients from the extract of *Euphorbia peplus*. Ingenol has been shown to bind and activate protein kinase C, and exhibits hepatic- and gastrointestinal-protective,[1] anti-tumor[2] and anti-HIV activities.[3] In particular, ingenol mebutate, a derivative of ingenol, has been successfully marketed as a licensed medicine for the treatment of actinic keratosis.[4–6] Considering that ingenol and its ingenane analogues have a variety of bioactivities, it is very significant to study the metabolic profiles of ingenol *in vivo* for clarifying and understanding efficacy and toxicity of ingenane diterpenoids.[7]

According to the guidance of the U.S. Food and Drug Administration (https://www.fda.gov/drugs/guidance-compliance-regulatory-information/guidances-drugs), drug metabolism is a very important part of safety evaluation and a major factor in drug development.[8–10] In recent years, the combination of a powerful analytical tool ultra-performance liquid chromatography-quadrupole time-of-flight-mass spectrometry (UPLC-Q/TOF-MS) and a computer-aided identification platform UNIFI (Waters® UNIFI® Scientific Information System), with the advantages of accuracy in mass measurement, high efficacy in separation technique and rapid identification in
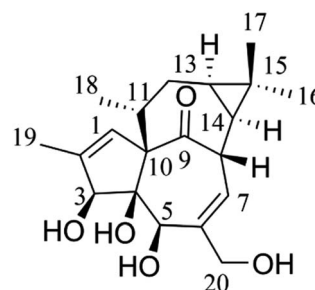
[a]*Department of Natural Medicinal Chemistry, School of Pharmacy, Naval Medical University, Shanghai 200433, China. E-mail: zuxianpeng@163.com; shenyunheng@hotmail.com*

[b]*School of Pharmaceutical Sciences, Yunnan Key Laboratory of Pharmacology for Natural Products, Kunming Medical University, Kunming 650500, Yunnan, China*

† Electronic supplementary information (ESI) available: The spectra including 1D, 2D-NMR, HRESIMS of compounds **2–4**. See DOI: 10.1039/d1ra07915h

‡ Si-Jia Xiao and Shan-Shan Li contributed equally to this work.

Fig. 1 The chemical structure of ingenol.

metabolites, has been widely applied for metabolic research.[11] However, there are still two major difficulties in the metabolite investigations. One is to obtain the accurate structures of metabolites, and the other is to obtain sufficient metabolites for further pharmacological and toxicological studies.[12] In order to solve these problems, it is essential to obtain the sufficient reference standards of metabolites. Generally, the preparation of metabolites mainly includes chemical methods,[12] small experimental animal models,[13] microsomal preparations,[9,14] enzyme-catalyzed reactions,[15,16] and microbial biotransformation,[12,17] *etc.* Compared with other methods, microbial biotransformation is more convenient and cost-effective, especially with the advantage of large-scale preparation *in vitro*.[17–21] Particularly, the fungus *Cunninghamella elegans* has been shown to possess the cytochrome P450 monooxygenase system similar to mammals, which could promote the reactions catalyzed by human CYP1A2, CYP2C9, CYP2C19, CYP2D6 and CYP3A4, thus producing similar metabolic profiles to mammals.[22,23] However, the presence and abundance of the metabolites determined by microbial transformation may not be an out-and-out representation of *in vivo* metabolites. Thus, a combination of these methods was applied in our study.

In this investigation, we aim to utilize UPLC-Q/TOF-MS and UNIFI platform to identify the metabolites of ingenol in rat, and to propose the metabolic pathways of ingenol. A total of 18 metabolites, including five phase II metabolites, were detected and identified. Hydroxylation, oxygenation, sulfonation, and glucuronidation were the predominant metabolic pathways of ingenol in rat. Additionally, microbial biotransformation based on the fungal strain *C. elegans* bio-110930 was applied to mimic and prepare metabolites of ingenol *in vivo*, so as to get more detailed metabolism information for predicting metabolites and interpreting structures of metabolites (Fig. 2).

Experimental section

Chemicals and reagents

Ingenol was purchased from Chengdu Herbpurify Co., Ltd. (Chengdu, China). Sabouraud dextrose broth was procured from Qingdao Hope Bio-Technology Co., Ltd. (cat no. HB0233, China). Sabouraud dextrose agar was obtained from Solarbio (cat no. P9240, China). The fungal strain, *C. elegans* (bio-110930), was purchased from the Beijing Baioubowei Biotechnology Co., Ltd. (Beijing, China). Column chromatography (CC) was performed using Sephadex LH-20 gel (GE Medical Systems Ltd, Buckinghamshire, U.K). Ethyl acetate and acetone were analytical grade from Shenyang Chemical Reagent Co., Ltd. (Shenyang, China). LC-MS-grade acetonitrile, methanol and formic acid were purchased from Fisher-Scientific (Fair Lawn, NJ, USA) and used in mobile phase and sample preparation. LC-MS-grade leucine enkephalin was obtained from Sigma-Aldrich (MO, USA). Ultra-pure water was purified by a Milli-Q system (Millipore, Bedford, MA, USA). All other reagents were of analytical reagent grade.

Instrumentation and analysis condition

For metabolite identification, chromatographic analyses were performed using a Waters Acquity UPLC I-class system (Waters, Milford, MA, USA), equipped with an auto-sampler, a binary solvent delivery system, an online degasser, and a photodiode array detector. An ACQUITY UPLC® HSS T3 column (2.1 mm × 150 mm, 1.8 μm, Waters) with a HSS T3 VanGuard™ Pre-Column 3/Pk (2.1 × 5.0 mm, 1.8 μm) was used. The optimized parameters were set as follows: the mobile phase consisted of eluent A (0.1% formic acid in water, v/v) and eluent B (acetonitrile). The flow rate was 0.3 mL min^{-1}. The column and auto-sampler temperatures were maintained at 40 °C and 4 °C, respectively. The gradient elution program was optimized as follows: 0–15 min, 5–90% B; 15–17 min, 90–100% B; 17–20 min, 100–100% B.

The mass spectrometry detection was performed on SYNAPT G2-Si HDMS system, equipped with an electrospray ionization (ESI) source (Waters Corp., Manchester, UK). Negative ion mode was conducted in this analysis. Mass spectrometry conditions were finally set as follows: capillary voltage 2.5 kV, cone voltage 40 V, source temperature 120 °C, and desolvation temperature 400 °C. Nitrogen was used as desolvation and cone gas with a flow rate of 800 and 50 L h^{-1}, respectively, and full-scan mass range was set as *m/z* 50–1500 Da. In auto mass spectrometry mode, the collision-induced dissociation energies were set at 5 eV for the precursor ion at low-energy mode, and the collision-induced dissociation energies were set from 20 to 40 eV for high-energy mode. Real-time data were calibrated using an external reference (LockSpray™) at a concentration of 0.2 ng mL^{-1} with an infusion flow rate of 10 μL min^{-1}, generating a reference ion for the negative ion mode (*m/z* 554.2615) during the UPLC-MS analysis. Data were acquired and processed using MassLynx™ NT 4.1 software (Waters, Milford, MA, USA).

Accurate molecular weights of some metabolites were acquired using an Agilent 6520 Accurate Mass quadrupole time-of-flight mass spectrometer (Q-TOF MS; Agilent Technologies, USA). The capillary voltage of the ion source was set at 3.5 kV in negative ion mode. Nitrogen was used as desolvation and nebulizing gas at a constant temperature of 350 °C. The scan range was set at *m/z* 100–1500 Da.

The isolation and purification of metabolites were performed using an Agilent 1200 series semi-preparative high performance liquid chromatography (HPLC) system (Palo Alto,
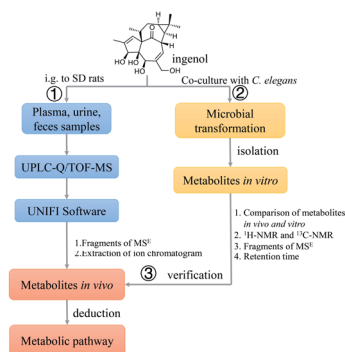

Fig. 2 A comprehensive strategy to systematically analyze the metabolites in rat of ingenol.

CA, USA) consisting of a G1311A quatpump solvent delivery system, G1379A degasser unit, a G1313A auto-sampler and a G1315B DAD detector. The preparation was performed with a Zorbax SB-C18 (5 μm, 9.4 mm × 25 cm) column (Agilent Technologies, US). The wavelength was set at 280 nm.

Nuclear magnetic resonance (NMR) spectra of ingenol and metabolites were measured on Bruker AV-500 spectrometers (Faellanden, Switzerland) using tetramethylsilane as internal standard.

Animals and drug administration

All animal procedures were performed in accordance with the Guidelines for Care and Use of Laboratory Animals of Naval Medical University and approved by the Animal Ethics Committee of Naval Medical University. Male Sprague–Dawley rats (200–250 g, Shanghai Sippr-BK Laboratory Animal Co., Ltd. (Shanghai, China, license no. SCXK-Shanghai-2018-0006)) were housed in humidity- and temperature-controlled room (50 ± 10% and 22–24 °C) with a 12 h light/dark cycle before the experiment. They were allowed free access to standard laboratory food and water for one week of acclimation, then fasted overnight but with free access to water before experiments. Ingenol was dissolved in 0.5% sodium carboxymethyl cellulose solution and then ultrasonically mixed for 30 min (10 mg mL^{-1}), and was administered orally to rats at the dose of 100 mg kg^{-1} body weight at a single dose.

Sample collection and preparation

Blood samples (0.5 mL) were collected from six rats through the orbital sinus before administration (blank sample) and 0.25, 0.5, 1, 2, 4, 6 and 12 h after administration. Plasma samples were prepared by centrifugation at 4000 rpm for 10 min. A 200 μL aliquot of plasma was mixed with four volumes of acetonitrile for protein precipitation and desalination. After centrifugation, the supernatant was transferred and evaporated to dryness under a nitrogen stream at 30 °C. The residue was re-dissolved in methanol (100 μL) and then was centrifuged at 4 °C and 12 000 rpm for 10 min. A 2 μL aliquot of the supernatant was injected into the UPLC-Q/TOF-MS system.

For urine and feces sampling, 12 rats were divided into administration group and blank group, and placed separately in stainless steel metabolic cages. Urine and feces samples were collected in containers surrounded by ice over 0–6, 6–12 and 12–24 hours before and after drug administration. The mix urine samples were centrifuged at 4000 rpm for 10 min at 4 °C, a 1 mL aliquot of supernatant was mixed with four volumes of acetonitrile. Feces samples (1.0 g) were crushed and then ultrasonically extracted by acetonitrile (10 mL) for 30 min. All the above-mentioned mixtures were centrifuged at 12 000 rpm at 4 °C for 10 min individually. The supernatants were transferred to clean tubes and evaporated to dryness at 30 °C under a gentle stream of nitrogen. The residues were dissolved in 100 μL of methanol and then centrifuged at 12 000 rpm at 4 °C for 10 min. A 1 μL aliquot of supernatants injected into the UPLC-Q/TOF-MS system for analysis.

Microbial transformation and isolation of ingenol

The biotransformation process was conducted using the fungus *C. elegans* bio-110930 at two scales: preliminary screening and preparative. Preliminary screening scale biotransformation of ingenol was carried out in 250 mL Erlenmeyer flasks containing 100 mL of liquid medium. The flasks were placed on a rotary shaker (160 rpm, 30 °C). A standard two-stage fermentation protocol was employed in all experiments.[24] After 2 days of pre-culture, the substrates 5 mg (dissolved in 0.5 mL acetone) were added into each flask. Taking 1 mL samples on days 0, 2, 4, 7, 10 and 14, samples were centrifuged and degree of transformation was compared to controls on TLC and UPLC-Q/TOF-MS. Culture controls consisted of sterile medium, in which microorganisms were grown under identical conditions without substrate. Substrate controls were composed of sterile medium and the same amount of substrate incubated under the same conditions without microorganisms.

The preparative scale biotransformation of ingenol by *C. elegans* bio-110930 was carried out in 50 Erlenmeyer flasks of 1000 mL (each flask containing 300 mL of medium), and autoclaved at 121 °C for 30 min. The flasks were inoculated with the fungal culture and placed on a shaker (160 rpm) at 28 °C for incubation. After 48 h of pre-culture, ingenol (1.0 g), dissolved in 50 mL acetone, was distributed among the 50 flasks evenly, and then left on a rotary shaker for another 7 days at 28 °C. Finally, the contents of all flasks were combined and filtered, and the aqueous layer was extracted three times with equal volumes of EtOAc. Then the organic layers were combined and evaporated under vacuum.

The crude extract (5.4 g) was eluted with gradient MeOH/H$_2$O (0–30% MeOH, 25 mL min^{-1}, 3 h; 30–50% MeOH, 25 mL min^{-1}, 3 h; 50–70% MeOH, 25 mL min^{-1}, 3 h; 70–100% MeOH, 25 mL min^{-1}, 3 h) on a Buchi reversed phase medium pressure liquid chromatography (RP-MPLC) instrument to yield 6 fractions (Fr. A–Fr. F). On the basis of TLC and HPLC analysis, the metabolites of ingenol were detected in Fr. B–Fr. E. Fr. B (131.4 mg) was separated on Sephadex LH-20 column chromatography (CC) (3 cm × 150 cm) with MeOH/H$_2$O (30%) to give Fr. B1–Fr. B5. Fr. B3 (22.3 mg) was purified by HPLC on a semi-preparative Zorbax SB-C18 column (CH$_3$CN/H$_2$O, 8%, 2 mL min^{-1}, 45 min) to give metabolites **M2** (4.5 mg, R_t = 37 min) and **M3** (5.8 mg, R_t = 40 min), Fr. D (2.13 g) was applied to Sephadex LH-20 CC (3 cm × 150 cm) with MeOH/H$_2$O (50%) to yield Fr. D1–Fr. D5, Fr. D2 (558.0 mg) was further subjected to Sephadex LH-20 CC (3 cm × 150 cm) to divide into five fractions (Fr. D2.1–Fr. D2.4). The metabolite **M4** (R_t = 36.0 min, 2.0 mg) were obtained by semi-preparative HPLC (CH$_3$CN/H$_2$O, 20%, 2 mL min^{-1}) from Fr. D2.2 (17.5 mg).

Results and discussion

Mass fragmentation behavior analyses of ingenol

For the purpose of obtaining a comprehensive fragmentation behavior of ingenol, the standard solution of ingenol was firstly analyzed *via* UPLC-Q/TOF-MS, which was helpful for the identification of ingenol metabolites.

The parent drug ingenol had a deprotonated molecular ion [M − H]$^-$ at *m/z* 347.1857 in negative ion mode. In the MS/MS spectrum, it had characteristic and the most abundant fragment ion at *m/z* 329.1766, derived from the loss of water, which
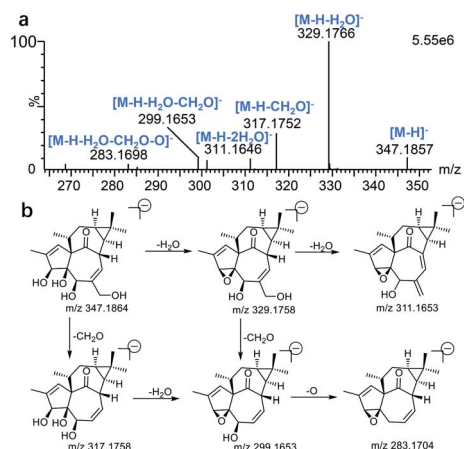
Fig. 3 The Mass spectrum (a) and proposed fragmentation pathways (b) of ingenol.

Table 2 The ^{13}C-NMR data for ingenol and its metabolites (M2−M4)

Position	Ingenol[a]	M2[a]	M3[a]	M4[a]
1	129.54 (d)	129.30 (d)	129.50 (d)	129.50 (d)
2	141.15 (s)	141.3 (s)	141.2 (s)	145.3 (s)
3	80.76 (d)	80.70 (d)	80.7 (d)	77.2 (d)
4	86.02 (s)	86.0 (s)	86.1 (s)	86.1 (s)
5	75.05 (d)	75.1 (d)	74.9 (d)	74.8 (d)
6	143.99 (s)	144.0 (s)	144.0 (s)	144.0 (s)
7	124.41 (d)	124.2 (d)	124.2 (d)	124.3 (d)
8	44.96 (d)	44.4 (d)	44.4 (d)	45.0 (d)
9	210.67 (s)	210.7 (s)	210.2 (s)	210.5 (s)
10	73.98 (s)	74.1 (s)	73.9 (s)	73.5 (s)
11	40.57 (d)	40.5 (d)	40.7 (d)	40.6 (d)
12	31.84 (t)	31.5 (t)	31.6 (t)	31.9 (t)
13	24.47 (d)	21.3 (d)	25.0 (d)	24.4 (d)
14	24.31 (d)	21.2 (d)	24.5 (d)	24.3 (d)
15	24.98 (s)	31.3 (s)	31.1 (s)	25.1 (s)
16	28.94 (q)	72.5 (t)	24.5 (q)	28.9 (q)
17	15.80 (q)	11.6 (q)	63.2 (t)	15.8 (q)
18	17.55 (q)	17.7 (q)	17.2 (q)	17.5 (q)
19	15.54 (q)	15.5 (q)	15.6 (q)	60.6 (t)
20	65.53 (t)	65.5 (t)	65.5 (t)	65.5 (t)

[a] Measured at 125 MHz in methanol-d_4.

further lost a water to form the ion at m/z 311.1646. The fragment ions at m/z 317.1752 and m/z 299.1648 were generated by loss of CH_2O from the fragments at m/z 347.1857 and m/z 329.1766, respectively. Moreover, the fragment at m/z 283.1698 resulted from the ion at m/z 299.1653 by loss of O. The loss of H_2O (m/z 329.1769) is the characteristic product ion of ingenol. Mass spectrum and the fragmentation scheme for ingenol are shown in Fig. 3. The ^{1}H-NMR and ^{13}C-NMR spectra data of ingenol are listed in Tables 1 and 2, with the carbon position labeled as shown in Fig. 1.

Structural elucidation of ingenol metabolites in rat

Total ion chromatograms of urine, feces and plasma samples, which were collected from the experimental rats after oral administration of ingenol, were analyzed by UNIFI 4.1 software. The analytes in each sample were compared according to the characteristic mass spectrum behavior (including parent ions, internal cleavage in the ion source, characteristic fragment ions of each metabolite) and retention time. Compared with the peaks in the corresponding blank sample, a total of 18 metabolites identified in rat are listed in Table 3. Extracted ion chromatograms and product ion spectra of metabolites are presented in Fig. 4 and 5. The proposed metabolic pathway of ingenol is shown in Fig. 6. The retention times, precursor molecular ion, key fragments, and distribution of ingenol and its metabolites are listed in Table 3.

Metabolites (M1–M4) were detected with the HPLC retention times between 4.34 and 6.93 min. The molecular ion at m/z

Table 1 The ^{1}H-NMR data of ingenol and its metabolites (M2−M4)

No.	Ingenol[a]	M2[a]	M3[a]	M4[a]
1	5.80 (q, 1.6)	5.79 (brd., 1.10)	5.81 (brd, 1.30)	6.08 (brt., 1.42)
3	4.34 (s)	4.35 (s)	4.34 (s)	4.54 (s)
5	3.63 (s)	3.65 (s)	3.63 (s)	3.68 (s)
7	5.96 (m)	6.00 (m)	5.98 (m)	5.97 (m)
8	4.28 (m)	4.32 (brd, 4.38)	4.42 (m)	4.30 (m)
11	2.42 (m)	2.48 (m)	2.44 (m)	2.48 (m)
12	2.38 (m)	2.40 (m)	2.47 (m)	2.41 (m)
	1.73 (dt, 6.30, 15.6)	1.74 (dt, 5.70, 15.30)	1.85 (m)	1.76 (m)
13	0.68 (td, 6.3, 8.7)	0.82 (td, 6.34, 8.56)	0.85 (m)	0.69 (m)
14	0.84 (dd, 8.4, 11.9)	1.00 (dd, 4.38, 8.56)	0.98 (dd, 6.79, 7.87)	0.85 (dd, 8.35,11.85)
16	1.06 (s)	3.26 (d, 11.18)	1.13 (s)	1.06 (s)
		3.24 (d, 11.18)		
17	1.12 (s)	1.18 (s)	3.74 (d, 11.64)	1.12 (s)
			3.70 (d, 11.64)	
18	0.94 (d, 7.10)	0.95 (d, 7.07)	0.95 (d, 7.09)	0.97 (d, 7.05)
19	1.82 (brd, 1.40)	1.82 (brd., 1.10)	1.82 (brd, 1.30)	4.23 (dd, 1.42, 14.65); 4.18 (dd, 1.65, 14.65)
20	4.10 (d, 13.6)	4.11 (d, 13.75)	4.10 (d, 13.35)	4.10 (d,13.70)
	4.04 (d, 13.20)	4.04 (d, 13.75)	4.03 (d, 13.35)	4.05 (d, 13.70)

[a] Measured at 500 MHz in methanol-d_4.

Table 3   Mass spectrum characteristics of metabolites of ingenol detected *in vivo* and *in vitro*

No.	Component Name	RT (min)	Formula $[M - H]^-$	Observed m/z	Error (ppm)	MS^n	Distribution Rat Blood	Urine	Faeces	Fungi
M1	M + O	4.34	$C_{20}H_{27}O_6$	363.1808	−1.38	363.1808, 345.1704, 333.1705, 327.1596, 319.1551, 315.1592, 309.1397, 297.1497	√	√	√	√
M2	M + O	5.00	$C_{20}H_{27}O_6$	363.1820	1.93	363.1820, 345.1726, 333.1720, 327.1608, 315.1610, 297.1501	√	√	√	√
M3	M + O	5.48	$C_{20}H_{27}O_6$	363.1808	−1.38	363.1808, 345.1709, 333.1704, 327.1594, 315.1597, 301.1803, 297.1490	√	√	√	√
M4	M + O	6.93	$C_{20}H_{27}O_6$	363.1804	−2.48	363.1804, 345.1698, 333.1700, 327.1591, 315.1594, 303.1591, 297.1492, 285.1487, 267.1384	√	√	√	√
M5	M + 2O	3.02	$C_{20}H_{27}O_7$	379.1776	3.69	379.1776, 361.1658, 349.1692, 343.1572, 331.1544, 301.1441	√	√	√	—
M6	M + 2O	3.63	$C_{20}H_{27}O_7$	379.1751	−2.90	379.1751, 361.1648, 349.1649, 343.1539, 331.1543, 313.1433, 319.1543, 301.1440, 283.1342	√	√	√	—
M7	M + 2O	3.82	$C_{20}H_{27}O_7$	379.1760	−0.53	379.1760, 361.1656, 349.1655, 343.1548, 331.1553, 319.1550, 313.1442, 301.1443, 283.1332	√	√	√	—
M8	M + 2O	3.94	$C_{20}H_{27}O_7$	379.1757	−1.32	379.1757, 361.1651, 349.1648, 343.1543, 331.1549, 313.1438, 301.1433, 283.1326	√	√	√	—
M9	M + 2O	4.30	$C_{20}H_{27}O_7$	379.1753	−2.37	379.1753, 361.1651, 349.1651, 343.1542, 331.1548, 319.1544, 313.1431, 301.1436, 283.1332	√	√	√	—
M10	M + O−2H	5.94	$C_{20}H_{25}O_6$	361.1643	−3.88	361.1643, 343.1542, 325.1442, 315.1600, 297.1495, 283.1484	√	√	√	—
M11	M + O−2H	6.34	$C_{20}H_{25}O_6$	361.1643	−3.88	361.1643, 343.1547, 325.1463, 315.1610, 297.1497	√	√	√	—
M12	M + 2O−2H	5.12	$C_{20}H_{25}O_7$	377.1593	−3.45	377.1593, 359.1500, 341.1387, 315.1591, 297.1487	√	√	√	—
M13	M + 2O−2H	5.82	$C_{20}H_{25}O_7$	377.1597	−2.39	377.1597, 359.1493, 341.1396, 315.1600, 297.1489	√	√	√	—
M14	M + SO₃	4.46	$C_{20}H_{27}O_8S$	427.1426	−1.40	427.1426, 345.1715, 327.1598, 315.1591, 297.1510, 285.1510, 79.9572	—	—	√	—
M15	M + SO₃	4.68	$C_{20}H_{27}O_8S$	427.1430	−0.47	427.1430, 345.1716, 327.1598, 315.1599, 79.9576	—	—	√	—
M16	M + SO₃	5.27	$C_{20}H_{27}O_8S$	427.1429	−0.70	427.1429, 345.1713, 327.1614, 315.1612, 79.9574	—	—	√	—
M17	M + $C_6H_8O_6$	6.88	$C_{26}H_{35}O_{11}$	523.2174	−2.10	523.2174, 345.1707, 315.1603, 297.1501, 175.0233	—	√	—	—
M18	M + $C_6H_8O_6$	7.08	$C_{26}H_{35}O_{11}$	523.2182	−0.57	523.2182, 345.1706, 315.1596, 175.0252	—	√	—	—

363.1808 ($[M - H]^-$) was observed, 16 Da mass of an oxygen atom more than that of ingenol. The fragment ions at m/z 345.1704 and m/z 327.1596 resulted from successive water loss from the ion at m/z 363.1808, and the fragment ions at m/z 333.1705, m/z 315.1592 and m/z 297.1497 were generated by CH_2O loss from m/z 363.1808, m/z 345.1704 and m/z 327.1596, respectively. The momohydroxylated products were more likely to lose a CH_2O group compared with ingenol. This clearly suggested that the hydroxylated site should be located on the methyl moiety of the molecule, but the exact substituted position remained to be determined.

The structure of **M2** was confirmed by comparison of its HPLC retention time and MS/MS fragments with the corresponding reference standard isolated and purified from microbial transformation samples (Fig. 7). The structure of **M2**

as the reference standard was determined based on NMR analyses. Tables 1 and 2 showed the comparison of the ^{1}H-NMR and ^{13}C-NMR data of metabolite **M2** and ingenol. The ^{1}H and ^{13}C-NMR spectroscopic data of **M2** displayed the resonances for structural fragments similar to those of ingenol, except that the appearance of an extra hydroxymethyl unit [δ_H 3.26 (d, 11.18) and 3.24 (d, 11.18); δ_C 72.5 (t)], instead of the methyl signals for C-16 in ingenol [δ_H 1.06 (s); δ_C 28.9 (q)], revealing that an additional hydroxyl group might be substituted at C-16 in **M2**. Furthermore, in the ^{13}C-NMR spectrum, the resonances of C-15 and C-16 were shifted significantly downfield from δ_C 24.98 to 31.3, and from δ_C 28.94 to 72.5, respectively, and the resonance of C-17 was shifted upfield from δ_C 15.8 to 11.6. As a result, the hydroxyl group was located at C-16. After browsing related research, **M2** was characterized as 16-hydroxyl ingenol by
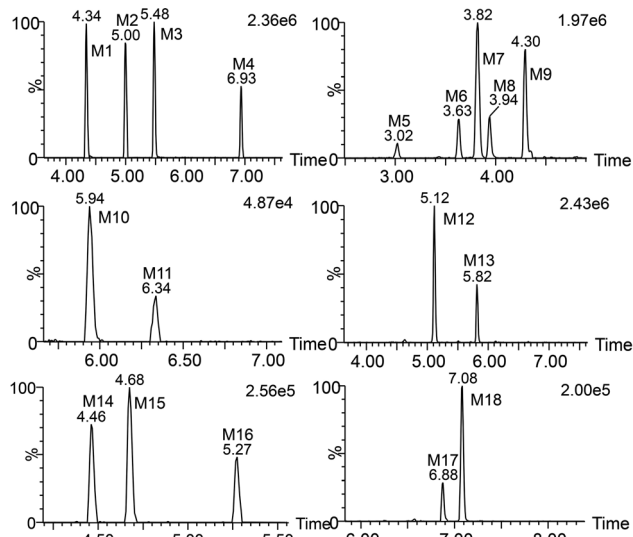
Fig. 4 Extracted ion chromatograms of ingenol metabolites in rat.

Fig. 6 The proposed metabolic pathway of ingenol in rat plasma (A), rat urine (B), rat feces (C), and micro-organism (D).

comparison of the NMR and HR-MS data with those of the literature.[25]

The structure of **M3** was confirmed by comparison of its HPLC retention time and MS/MS fragments with the corresponding reference standard isolated and purified from microbial transformation products (Fig. 7). Analysis of the ^{1}H and ^{13}C-NMR spectroscopic data of **M3** revealed structural similarity to ingenol (Tables 1 and 2), the appearance of an extra oxygenated methylene unit [δ_H 3.74 (d, $J = 11.64$ Hz, H-17a) and 3.70 (d, $J = 11.64$ Hz, H-17b); δ_C 63.2], in place of the methyl signals for C-17 (δ_H 1.12; δ_C 15.8) in ingenol, suggesting the introduction of one additional hydroxyl group in **M3**. In addition, the resonance of C-15 appeared at lower field at δ_C 31.1 and C-16 was shifted upfield to δ_C 24.5. Consequently, the extra
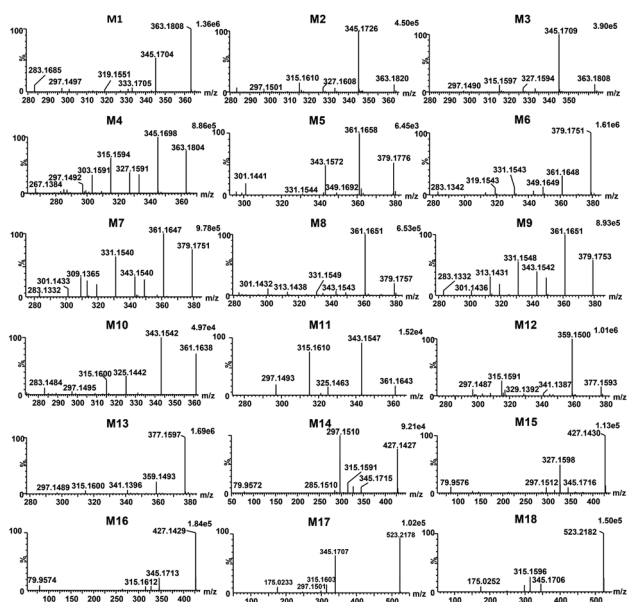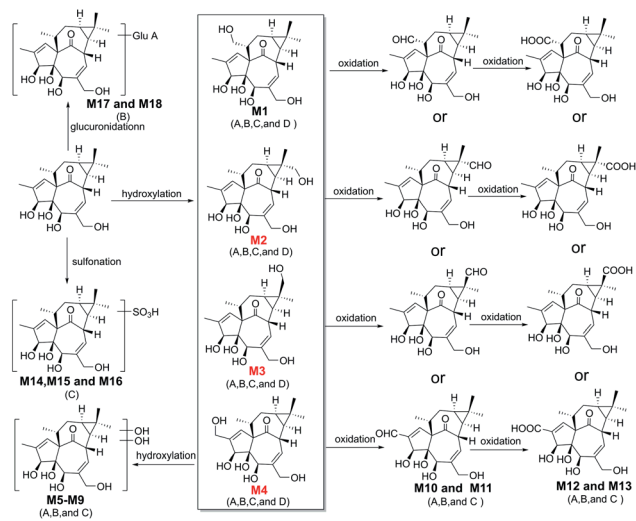
hydroxyl group was attributed to C-17, which was further evidenced by key HMBC correlations from the hydroxymethylene protons at δ_H 3.74 and 3.70 to C-13, C-14, and C-15, and from H-16 at δ_H 1.13 to C-13, C-14, C-15 and C-17, together with key NOESY correlations of the hydroxylmethyl protons at δ_H 3.74 and 3.70 with H-8 (δ_H 4.42) and H-12 at δ_H 2.47 (Fig. S1†). Therefore, **M3** was assigned as 17-hydroxyl ingenol.

The structure of **M4** was confirmed by comparing the HPLC retention time and MS/MS fragments of **M4** with the corresponding reference standard isolated and purified from microbial transformation products (Fig. 7). The ^{1}H-NMR spectrum of **M4** (Table 1) displayed characteristic signals of only

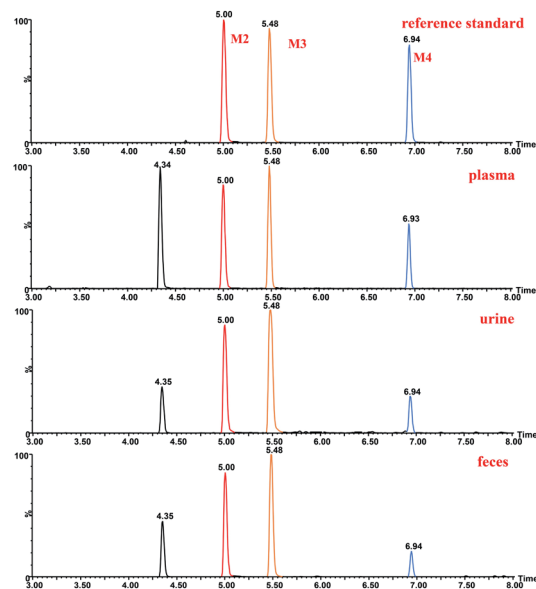Fig. 5 Product ion spectra of ingenol metabolites in rat.

Fig. 7 Extracted ion chromatograms of ingenol metabolites in rat and reference standard isolated and purified from microbial transformation samples.

three methyls H-16 (δ_H 1.06), H-17 (δ_H 1.12) and H-18 (δ_H 0.97), with two extra oxygenated protons at δ_H 4.23 (dd, J = 1.42, 14.65 Hz) and δ_H 4.18 (dd, J = 1.65, 14.65 Hz), rather than four methyl groups of ingenol, indicating that a methyl was hydroxylated in **M4**. Compared to the ^{1}H-NMR and ^{13}C-NMR spectra of ingenol (Tables 1 and 2), the signals for a hydroxymethylene occurred at δ_C 60.6 in ^{13}C-NMR spectrum and at δ_H 4.23 (dd, J = 1.42, 14.65 Hz) and δ_H 4.18 (dd, J = 1.65, 14.65 Hz) in ^{1}H-NMR spectrum in **M4**, instead of the methyl signals for C-19 at δ_H 1.82 (brd, 1.40) and δ_C 15.5 in ingenol, suggesting the additional hydroxyl group to be attached to C-19. This coincided with the ^{13}C-NMR resonances observed for downfield shift of C-2 ($\Delta\delta$ + 4.15) and upfield shift of C-3 ($\Delta\delta$ − 3.56) in comparison with those of ingenol. Furthermore, the HMBC correlations of H-19 (δ_H 4.23 and 4.18) with C-1, C-2 and C-3, revealing the hydroxylation of C-19. Thus, **M4** was established as 19- hydroxyl ingenol.

Due to the fragment pathway, the hydroxyl groups of metabolites **M1–M4** were substituted on the methyl groups of ingenol. The hydroxyl groups of metabolites **M2–M4** occupied at C-16, C-17 and C-19, respectively. Only a methyl group at C-18 was not replaced, therefore, metabolite **M1** was most likely to be hydroxylated at the remaining methyl group of ingenol.

Metabolites **M5–M9** were predicted to be dihydroxylated derivatives with HPLC retention times between 3.02 and 4.30 min. Their parent ions were detected at m/z 379.1751 ([M − H]$^-$) in negative ion mode, 16 mass unit more than those of **M1–M4**, suggested the presence of an additional hydroxyl group. The fragment ions at m/z 361.1648 and m/z 343.1539 resulted from successive water loss of the fragment ion at m/z 379.1751, and the fragment ions at m/z 349.1649, m/z 331.1543 and m/z 313.1433 were generated by CH_2O loss from the fragment ions at m/z 379.1751, m/z 361.1648 and m/z 343.1539, respectively. The fragment ions at m/z 331.1553 and m/z 313.1442 also resulted from successive H_2O loss of the fragment ion at m/z 349.1649. In particular, the fragment ions at m/z 349.1649 and 319.1543 were generated by successive CH_2O loss of the ion at m/z 379.1751, in which the ions at m/z 283.1342 and 313.1433 resulted from the ion at m/z 343.1539 in similar mechanism. Consistent with monohydroxylation products of ingenol, they showed a series of product ions resulting from loss of H_2O and CH_2O. More fragments resulted from loss of CH_2O, demonstrating that dihydroxylated ingenol metabolites had more hydroxyl groups at methyl moiety than monohydroxylated metabolites.

Metabolites (**M10–M11**) were detected 5.94 and 6.34 min. The parent ion was detected at m/z 361.1643 ([M − H]$^-$) in negative ion mode. They were 14 Da more than ingenol and 2 Da less than **M1–M4**, which were hydroxylation products of ingenol. The fragment ions at m/z 325.1442 and 343.1542 were generated by successive water loss from the ion at m/z 361.1643. The fragment ions at m/z 315.1600 and 297.1495 were generated by CO loss from the ions at m/z 343.1542 and m/z 325.1442, respectively, indicating the existence of an aldehyde group. Furthermore, according to the proposed metabolic pathway of tanshinone IIA by Sun et al.,[26] the metabolic modification could take place in the methyl of ingenol, from methyl to primary alcohol, then to aldehyde group. Thus, it is provisionally interpreted that **M10** and **M11** was produced by transforming methyl of ingenol to aldehyde.

Metabolites (**M12–M13**), which showed deprotonated ion at m/z 377.1593 ([M − H]$^-$) in negative ion mode with the retention times of 5.12 and 5.82 min, were 30 Da more than ingenol and 2 Da less than dihydroxylation products of ingenol like **M5–M9**. The fragment ions at m/z 359.1500 and 341.1387 were proposed to result from successive loss of water from the molecular ion at m/z 377.1593. In addition, the fragments at m/z 315.1591 and m/z 297.1487 were generated from the ions at m/z 359.1500 and m/z 341.1387 following loss of CO_2, respectively. The fragment spectrum showed a prominent loss of CO_2, indicating the existence of carboxyl group. This compound might be produced by the oxidation of **M10** or **M11**, which was further in accordance with our initial speculation. Therefore, it is provisionally interpreted that **M12** and **M13** was produced by transforming aldehyde of **M10** or **M11** to carboxyl.

Metabolites (**M14–M16**) were detected at HPLC retention times between 4.46 and 5.27 min. They showed a molecular ion at m/z 427.1426 ([M − H]$^-$) in negative ion mode, with 80 Da more than ingenol. The fragment ion at m/z 345.1715 provided reliable evidence for identifying metabolites, and molecular ion of SO_3 at m/z 79.9576 ([M − H]$^-$) was also observed, demonstrating that a hydroxyl group in ingenol was replaced by SO_3. Therefore, they were tentatively identified as sulfonated products of ingenol.

Metabolites (**M17** and **M18**) eluted at about 6.88 and 7.08 min, respectively. They gave the deprotonated molecule ion [M − H]$^-$ at m/z 523.2174, 176 Da more than ingenol. The fragment ion at m/z 345.1707 was proposed to result from loss of $C_6H_{10}O_6$ from the molecular ion, and the deprotonated ion [M − H]$^-$ of $C_6H_8O_6$ at m/z 175.0233 was also observed, indicating a hydroxyl group of ingenol was replaced by a glucruonide.

Elucidation of the metabolic pathway in rat

In vivo metabolism of ingenol and the metabolic pathways were accordingly proposed using UPLC-Q/TOF-MS, as shown in Fig. 6. In general, the *in vivo* metabolism of ingenol can be concluded to undergo four pathways. The first pathway is hydroxylation of methyl moiety to form monohydroxylated ingenol (**M1–M4**), which undergo further metabolism to form dihydroxylated ingenol (**M5–M9**). The second pathway involves the oxidation of methyl in ingenol, from methyl to primary alcohol, then to aldehyde group (**M10–M11**), and finally to carboxyl group (**M12–M13**). The third metabolic pathway is the direct sulfonation of the hydroxyl part in ingenol to form sulfonated adducts (**M14** and **M16**). The fourth metabolic pathway is to directly combine with glucuronide to form glucuronide adducts (**M17** and **M18**). Therefore, hydroxylation, oxidation, sulfonation and glucuronidation are the main metabolic pathways of ingenol in rat.

In addition, in this study, phase I metabolites were detected in rat plasma, urine and feces, while phase II metabolites were detected only in urine or feces. Therefore, phase I metabolites of ingenol might be potential components with pharmacological or toxicological effects,[27] and phase II metabolites usually increase polarity and reduce liposolubility, so as to accelerate drug excretion from the body and usually play a detoxification role in drug metabolism.[28]

Conclusions

In the present study, a rapid and reliable analytical method based on UPLC Q/TOF-MS was developed and used for the identification of ingenol metabolites in rat (plasma, urine, and feces) and *C. elegans* bio-110930 model. A total of 18 metabolites were identified *in vivo* based on the molecular ions and the MS/MS fragments, including monohydroxylated ingenol (**M1–M4**), dihydroxylated ingenol (**M5–M9**), methyl hydroformlated ingenol (**M10** and **M11**), methyl carboxylated ingenol (**M12** and **M13**), sulfate ingenol (**M14–M16**) and glucuronide ingenol (**M17** and **M18**). Among them, reference standards of three metabolites were further prepared by preparative scale microbial transformation. The structures of these metabolites were confirmed by comparison of their HPLC retention times and MS/MS fragments with the prepared reference standards, whose structures were determined based on 1D and 2D NMR analyses. The three identified metabolites were 16α-hydroxy ingenol (**M2**), 17β-hydroxy ingenol (**M3**), and 19-hydroxy ingenol (**M4**). Furthermore, ingenol was proved to be metabolized mainly *via* hydroxylation, oxygenation, sulfonation, and glucuronidation. Moreover, *C. elegans* bio-110930 could be a suitable model to simulate and prepare ingenol phase I metabolites. Thus, an overall description of metabolites of ingenol from rat and *C. elegans* bio-110930 has been provided. Furthermore, our study provides valuable information in predicting *in vivo* human metabolites of ingenol.

Conflicts of interest

There are no conflicts to declare.

Acknowledgements

Notes and references

1 Z. Qiao, H. J. Yong, Z. Yi, W. Kan, Z. Min, D. C. Pei, F. Y. Wei, P. T. Yu, H. W. Jian and Z. Li, *J. Ethnopharmacol.*, 2020, **267**, 113507.

2 C. M. Hasler, G. Acs and P. M. J. C. R. Blumberg, *Cancer Res.*, 1992, **52**, 202–208.

3 K.-J. Hong, H. S. Lee, Y.-s. Kim and S. S. Kim, *Public Health Res. Perspect.*, 2011, **2**, 109–114.

4 A. K. Gupta and M. Paquet, *J. Cutaneous Med. Surg.*, 2013, **17**, 173–179.

5 D. R. Alchin, *Dermatol. Ther.*, 2014, **4**, 157–164.

6 M. Bourcier, L. Stein Gold, L. Guenther, C. M. Andreassen, J. Selmer and G. Goldenberg, *J. Dermatol. Treat.*, 2017, **28**, 652–658.

7 I. P. de Sousa, M. V. Sousa Teixeira and N. A. Jacometti Cardoso Furtado, *Molecules*, 2018, **23**, 1387–1419.

8 F. P. Guengerich, *Chem. Res. Toxicol.*, 2009, **22**, 237–238.

9 F. Gaunitz, P. Dahm, L. Mogler, A. Thomas, M. Thevis and K. Mercer-Chalmers-Bender, *Anal. Bioanal. Chem.*, 2019, **411**, 3561–3579.

10 K. E. Grafinger, A. Wilke, S. Knig and W. Weinmann, *Drug Test. Anal.*, 2019, **11**, 721–729.

11 L. Xu, Y. Liu, H. Wu and A. Zhou, *J. Chromatogr. B: Anal. Technol. Biomed. Life Sci.*, 2019, **1137**, 121934.

12 K. Li, F. Qin, L. Jing, F. Li and X. Guo, *Anal. Bioanal. Chem.*, 2013, **405**, 2619–2634.

13 M. Duan, Q. Li, D. Zhong and Z. Peng, *J. Chromatogr. B: Anal. Technol. Biomed. Life Sci.*, 2018, **1095**, 138–141.

14 R. He, J. Fan, R. Chen, D. Guo, M. Zhao, Z. Zhang, C. Liang, M. Chen, H. Song and W. Zhang, *Chemosphere*, 2021, **264**, 128495.

15 T. Nguyen, S.-J. Yeom and C.-H. Yun, *Appl. Sci.*, 2021, **11**, 603–626.

16 K. Lapham, E. Callegari, J. Cianfrogna, J. Lin, M. Niosi, C. C. Orozco, R. Sharma and T. C. Goosen, *Drug Metab. Dispos.*, 2020, **48**, 1350–1363.

17 Y. Ma, P. Sun, Y. Zhao, K. Wang, X. Chang, Y. Bai, D. Zhang and L. Yang, *Molecules*, 2019, **24**, 315–328.

18 K. Yildirim, A. Kuru and E. Küçükbaşol, *Biocatal. Biotransform.*, 2019, **38**, 7–14.

19 A. Aziz, S. Bano, W. Atia Tul and M. I. Choudhary, *Steroids*, 2020, **154**, 108467.

20 R. Sponchiado, J. M. Sorrentino, N. Olegario, S. S. Oliveira, L. M. Cordenonsi, G. P. Silveira, A. M. Fuentefria, A. S. L. Mendez, M. Steppe and C. V. Garcia, *Biomed. Chromatogr.*, 2019, **33**, e4496.

21 C. Chen, K. Song, Y. Zhang, C. Chu, B. Fan, Y. Song, H. Huang and G. Chen, *Phytochemistry*, 2021, **182**, 112608.

22 W. Palmer-Brown, R. Miranda-CasoLuengo, K. H. Wolfe, K. P. Byrne and C. D. Murphy, *Sci. Rep.*, 2019, **9**, 9240–9248.

23 S. Asha and M. Vidyavathi, *Biotechnol. Adv.*, 2009, **27**, 16–29.

24 Y. Wang, L. Xiang, Z. Wang, J. Li, J. Xu and X. He, *Bioorg. Chem.*, 2020, **101**, 103870.

25 J. B. He, H. J. Zhu, G. F. Luo, G. M. Liu, Y. Li, H. Chen, S. P. Chen, X. Lu, G. C. Zhou and Y. X. Cheng, *Bull. Korean Chem. Soc.*, 2010, **31**, 2211–2214.

26 J. H. Sun, M. Yang, X. M. Wang, M. Xu, A. H. Liu and D. A. Guo, *J. Pharm. Biomed. Anal.*, 2007, **44**, 564–574.

27 U. M. Zanger and M. Schwab, *Pharmacol. Ther.*, 2013, **138**, 103–141.

28 Z. Zhang and T. Wei, *Acta Pharm. Sin. B*, 2018, **8**, 721–732.